AIAA JOURNAL
Vol. 44, No. 12, December 2006

Dynamics of a Three-Dimensional Oscillating Foil Near the Free Surface

Qiang Zhu*
University of California, San Diego, La Jolla, California 92093-0085
and
Yuming Liu† and Dick K. P. Yue‡
Massachusetts Institute of Technology, Cambridge, Massachusetts 02139

DOI: 10.2514/1.21617

We investigate the free-surface effects on an underwater three-dimensional foil undergoing constant translation and periodic oscillation using a hybrid computational method. In this approach, the fluid motion around the foil is modeled via boundary-integral formulation, and the shed vorticity is represented as a shear layer originated from the trailing edge, while the free-surface waves are resolved by a spectral algorithm. We apply this method to investigate the hydrodynamic forces and free-surface wave signatures of two canonical problems of oscillating foils with forward speed: a horizontal foil undergoing heaving motion and a vertical foil in sway motion. In the horizontal-foil case, we find that the solution has a strong dependence on the unsteady parameter. Near the critical value, the mean thrust and the propulsive efficiency of the foil are significantly reduced, and the free-surface wave field is dominated by the unsteady waves produced by the oscillatory motion rather than the steady Kelvin waves due to forward motion. The surface waves induced by the wake vortices appear as a sequence of ringlike patterns along the track. In contrast, for the swaying vertical foil, the hydrodynamic forces vary smoothly near τ_c, while the wake-induced waves exhibit the characteristic meandering feature.

Nomenclature

C_l	=	lift coefficient
C_t	=	mean thrust coefficient
c	=	chord length of the foil
d	=	submergence (draft)
$\boldsymbol{F}$	=	total hydrodynamic force on the foil
$\bar{F}$	=	mean thrust force in the direction of U
F_r	=	$U/\sqrt{gc}$ Froude number
f	=	$\omega/2\pi$
g	=	gravitational acceleration
h	=	amplitude of heaving/swaying motion
S_b	=	body surface
S_f	=	free surface
S_t	=	$2fh/U$ Strouhal number
$\bar{S}_f$	=	mean free surface
S_w	=	wake sheet
s	=	span length of the foil
t	=	time
U	=	forward speed
x, y, z	=	Cartesian coordinates
ζ	=	free-surface elevation
η	=	propulsion efficiency
ρ	=	density of fluid
τ	=	$U\omega/g$ unsteady parameter
τ_c	=	0.25, critical value of τ
Φ	=	velocity potential
ϕ_b	=	velocity potential caused by the body
ϕ_f	=	velocity potential caused by the free surface
ϕ_w	=	velocity potential caused by the wake
ω	=	frequency of oscillation

Received 8 December 2005; revision received 29 May 2006; accepted for publication 18 July 2006.

*Assistant Professor, Department of Structural Engineering; qizhu@ucsd.edu.
†Principle Research Scientist, Department of Mechanical Engineering.
‡Professor, Department of Mechanical Engineering.

I. Introduction

INVESTIGATIONS in unsteady propulsion using flapping foils, motivated by caudal fins of fish or wings of birds, have shown the ability of such motions to obtain high propulsion efficiencies [1–3] and large transient forces [4]. In addition to propulsion, and low-speed maneuvering and stabilization, many recent applications have been found for such flapping foils, among them a novel foil-based windmill that can harvest energy from currents [5].

The dynamics and near-body flowfield around an oscillating foil have been investigated extensively through experiments [3,4,6], theoretical analysis [1,7,8], and computational simulations [9–11]. All of them, however, are in the context of operation in an unbounded fluid. When the flapping foil is operating close to the water surface, the foil itself, together with the vortex wake shed from it, may interact strongly with the free surface. The dynamic behavior of the foil may differ significantly from that in an unbounded fluid. In addition, the resulting wave patterns or signatures on the free surface may possess unique characters.

The investigation of the free-surface effects on submerged foils has been focused in the two-dimensional steady problems. In the context of potential flow, the linear interaction between a two-dimensional thin hydrofoil and a free surface has been studied both theoretically [12] and numerically [13,14]. The second-order effect of the free surface has also been examined [15,16]. The fully nonlinear wave-body vortex interaction was investigated by Tsai and Yue [17], who employed a fully nonlinear mixed-Eulerian–Lagrangian approach to study the dynamics of a near-surface vortex sheet shed from the bottom of a moving surface-piercing strut. They found that the dynamics of the problem is governed by a single parameter $F_n = U/\sqrt{gd}$, where d is the draft of the strut. For $F_n > 1$, strong vortex-wave coupling is observed while their interinfluences are not significant in other cases. Chen and Chwang [18] examined the viscous effects in the problem of a steady translation of a submerged foil using a Navier–Stokes equations solver and found that the presence of a free surface influences the frequency of vortex shedding at given Reynolds numbers.

The study of the effects of unsteady foil motions and three dimensionality of foil geometry is quite limited. To illustrate the

effect of unsteady foil motions, Grue et al. [19] studied the linear problem of a two-dimensional flat plate near the free surface using a frequency-domain integral equation approach. Their work focused on energy harvesting from incoming waves by a thrust-generating foil and demonstrated the capability of converting wave energy into thrust in both head and following seas in agreement with the experiments of Isshiki et al. [20]. For the three-dimensional problem, Bal et al. [21] developed a hybrid boundary-element method and applied it to simulate the dynamics of a cavitating foil near the free surface. The motion of the foil is assumed to be steady, and the unsteady motion is not considered.

In this work, we address the general three-dimensional problem in which a three-dimensional foil undergoes an arbitrary motion in or near the free surface. The fully coupled interactions among the foil, the shed vortex in the wake, and the surface waves are considered. An efficient three-dimensional hybrid numerical algorithm is developed to resolve this problem. In this approach, we use a boundary-element method [22] for the fluid flow around the body. The wakes, originating from sharp trailing edges on the body, are modeled as shear layers, or, equivalently, normal dipole distributions on thin sheets. To account for the large geometric nonlinearity introduced by the arbitrary motion of the foil, we adopt a body nonlinear formulation in which the body boundary condition is satisfied exactly at the instantaneous surface of the body. The linear free-surface effects are accounted for by using a highly efficient pseudospectral algorithm. This method achieves exponential convergence with respect to the number of free-surface modes and requires a (approximately) linear computational cost with the number of unknowns. Depending on the wave steepness, free-surface nonlinearity may play an important role in the problem especially when the foil operates very close to the free surface, or in the presence of large-amplitude ambient surface waves. These situations are excluded from the present study.

Combining the boundary-element method and the spectral approach, our hybrid method is capable of simulating submerged bodies with arbitrary geometries, including those with sharp trailing edges where vortices are shed. The accuracy and efficiency of the spectral method provides high resolution of the free-surface disturbances due to the body and the wake vortices. Furthermore, the computational efficiency of the spectral method allows us to carry out simulations in large domains and resolve detailed wave features in the far field.

With this hybrid method, we perform numerical investigations of the dynamics of three-dimensional oscillating foils near the free surface. For illustration, we consider two canonical cases involving foils with steady forward speed while undergoing sinusoidal oscillating motion. First, we study a heaving rectangular-shaped NACA0012 foil with its midplane parallel to the mean free surface (horizontal-foil case). The dimensionless parameters involved in this problem are the aspect ratio of the foil, the submergence-to-chord ratio, the Froude number, the amplitude-to-chord ratio, and the unsteady parameter $\tau \equiv U\omega/g$. For shallow submergence and τ near the critical value $\tau_c \equiv 0.25$, we find a distinctive free-surface effect on the thrust and propulsion efficiency of the foil accompanied by the generation of large unsteady waves. We contrast this case to the one where the midplane of the foil is perpendicular to the mean free surface and undergoing sway motion (vertical-foil case). The influence of the free surface is generally much less significant in this case. The strong τ_c influence is not observed in either the mean thrust or the propulsion efficiency.

Depending on the kinematic parameters, the foil creates either a Kármán vortex street (drag wake), or a reverse Kármán vortex street (thrust wake), in its wake consisting of two arrays of vortices shed from the trailing edge. In the horizontal-foil case, the vortex array closer to the free surface produces a sequence of ringlike surface features along the track. In the vertical-foil case, the two arrays of vortices together create a free-surface pattern consisting of meandering ringlike waves.

The rest of the paper is organized as follows. In Sec. II, we give a brief description of the physical problem. The mathematical formulation is provided in Sec. III, while in Sec. IV the key numerical issues about the hybrid algorithm, including the implementation and validation of the numerical solver, are discussed. In Sec. V, this method is applied to study the hydrodynamic behavior and wave generation of near-surface horizontal and vertical foils. Conclusions are drawn in Sec. VI.

II. Problem Description

We consider the unsteady motion of a three-dimensional submerged, rectangular NACA0012 foil, with span s and chord c, operating in deep water. The flowfield, bounded by the free surface and the foil surface, is assumed to be incompressible and irrotational, except for the (infinitesimally) thin wake shed from the trailing edge of the foil. We employ a space-fixed Cartesian coordinate system (x, y, z), with the origin in the mean free surface, x and y the horizontal coordinates, and z positive pointing upward.

The foil moves in the $-x$ direction with constant speed U, while at the same time undergoes an oscillating motion. Two types of foil and motion configurations are considered. The first one is a heaving motion of a horizontal foil (Fig. 1). The heaving motion is prescribed as $z(t) = h\sin(\omega t)$. The second problem we consider is the swaying motion of a foil with its span perpendicular to the free surface (Fig. 2). The swaying motion $y(t)$ is given by $y(t) = h\sin(\omega t)$.

In the framework of a potential flow, we impose a Kutta condition at the sharp trailing edge of the foil that requires the flow to leave the trailing edge smoothly with finite speed. At any instant, the fluids leaving the upper and lower faces of the trailing edge, generally with different speeds, create a zero-thickness shear layer behind. This wake sheet subsequently evolves and is advected and deformed by the fluid velocity in the wake. The dynamics of the system is affected by interactions with the free surface on which the kinematic and dynamic free-surface boundary conditions apply. Consequently, the free-surface disturbance, the pressure distribution on the foil surface, and the shed wake are coupled. In addition to the free-surface effect on the foil dynamics, the foil and the presence and evolution of the vorticity wake create distinctive surface features which are substantially more complicated than the classical Kelvin ship waves or the unsteady ship waves generated by an oscillating forward moving body [23].

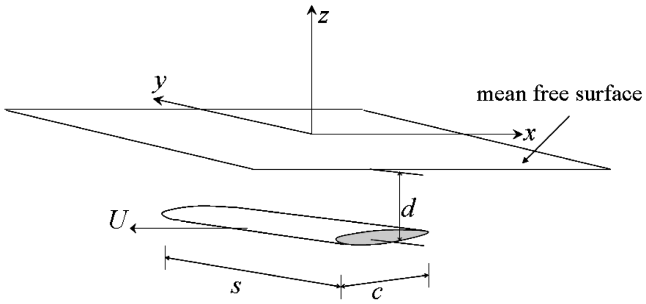

Fig. 1 Schematic of a horizontal foil submerged under the free surface.

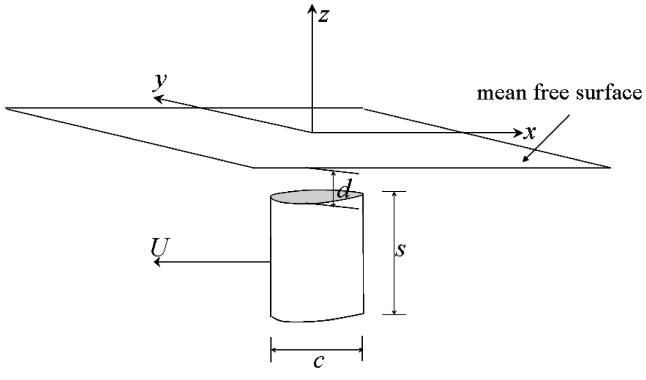

Fig. 2 Schematic of a vertical foil submerged under the free surface.

III. Mathematical Formulations

A. Initial Boundary-Value Problem

We define a velocity potential $\Phi(\boldsymbol{x}, z, t)$ where $\boldsymbol{x} \equiv (x, y)$ is the horizontal coordinate. At any instant, Φ satisfies the Laplace equation in the fluid domain and the linearized kinematic and dynamic free-surface boundary conditions at the mean free surface $\bar{S}_f$:

$$\left.\begin{aligned} \zeta_t - \Phi_z = 0 \\ \Phi_t + g\zeta = 0 \end{aligned}\right\} \tag{1}$$

where $\zeta(\boldsymbol{x}, t)$ represents the free-surface elevation.

On the instantaneous surface of the foil $S_b(t)$, the no-flux condition is imposed

$$\boldsymbol{n} \cdot \nabla\Phi = \boldsymbol{n} \cdot \boldsymbol{V}_b(\boldsymbol{r}, t) \tag{2}$$

where $\boldsymbol{n}$ is the unit normal vector which points into the fluid, $\boldsymbol{r} = (x, y, z)$, and $\boldsymbol{V}_b$ is the specified instantaneous velocity of the body. At the sharp trailing edge, the Kutta condition is imposed such that the flow leaves the edge smoothly. As initial conditions at $t = 0$, the body position S_b, the body velocity $\boldsymbol{V}_b$, the free-surface elevation ζ, and the velocity potential Φ on the free surface are specified. For computations, we impose doubly periodic boundary conditions on the horizontal plane so that the problem is periodic in both x and y with periods of $2L$ and $2W$, respectively.

In solving this initial boundary-value problem, two key steps of operations are usually involved at any time t: 1) with the velocity Φ_z on the mean free surface determined from the boundary-value problem solution, integrate the evolution Eq. (1) forward in time to obtain new values of the free-surface elevation and velocity potential at $t + \Delta t$, and 2) solve the boundary-value problem to obtain the velocity on the mean free surface and the pressure distribution on the body. The complete solution of the problem is obtained by repeating these processes starting from $t = 0$. Between these two processes, step 2 is the key.

B. Problem Decomposition

In solving the boundary-value problem, we write the total potential Φ as a linear superposition of three parts, $\Phi = \phi_b + \phi_w + \phi_f$, where ϕ_b represents the contribution from the foil body, ϕ_w the contribution from the wake, and ϕ_f the influence of the free surface. Following Zhu et al. [22], we decompose the body-wake-surface interaction problem for Φ into three coupled boundary-value problems for ϕ_b, ϕ_f, and ϕ_w.

For the body influence problem for ϕ_b, we assume that ϕ_w and ϕ_f are given and apply the no-flux boundary condition (2) to determine ϕ_b. Similarly, we formulate the free-surface problem for ϕ_f as a Dirichlet problem by specifying the value of ϕ_f at the mean free surface (with $\phi_f = \Phi - \phi_b - \phi_w$). Finally, we model ϕ_w as the induced velocity potential of a zero-thickness shear layer in the wake. This layer originates from the sharp trailing edge of the foil. At each instant, the strength of the newly created potion of the layer is determined by the Kutta condition at the trailing edge, provided that ϕ_b and ϕ_f are known. The rest of the layer is allowed to be advected downstream by the combined velocity field of ϕ_b, ϕ_f, and ϕ_w.

In the following, a detailed description of the formulation for each of these three problems is described.

1. *Boundary-Integral Equation for ϕ_b*

At any time t, if ϕ_w and ϕ_f are given, ϕ_b is determined by implementing the boundary condition (2), which is rewritten as

$$\boldsymbol{n} \cdot \nabla\phi_b = \boldsymbol{n} \cdot [\boldsymbol{V}_b(\boldsymbol{x}, z, t) - \nabla\phi_w - \nabla\phi_f] \tag{3}$$

Upon invoking Green's theorem, we have

$$2\pi\phi_b(\boldsymbol{r}, t) + \iint_{S_b} \phi_b(\boldsymbol{r}', t)\boldsymbol{n} \cdot \nabla G(|\boldsymbol{r} - \boldsymbol{r}'|)\, \mathrm{d}s' = \iint_{S_b} G(|\boldsymbol{r} - \boldsymbol{r}'|)\boldsymbol{n} \cdot \nabla\phi_b(\boldsymbol{r}', t)\, \mathrm{d}s' \tag{4}$$

for any $\boldsymbol{r} = (x, y, z)$ on the foil surface ($\boldsymbol{r} \in S_b$), where G is a doubly periodic Green function:

$$\begin{aligned} G(\boldsymbol{r} - \boldsymbol{r}') = G(\boldsymbol{r} - \boldsymbol{r}' + 2nL\boldsymbol{i} + 2lW\boldsymbol{j}) \\ n, l = 0, \pm 1, \pm 2, \ldots, \pm\infty \end{aligned} \tag{5}$$

where $\boldsymbol{i}$ and $\boldsymbol{j}$ are unit vectors in the x and y directions, respectively. In terms of Rankin sources, G can be expressed in the form:

$$G(\boldsymbol{r} - \boldsymbol{r}') = \sum_{n=-\infty}^{\infty} \sum_{l=-\infty}^{\infty} [|\boldsymbol{r} - \boldsymbol{r}' + 2nL\boldsymbol{i} + 2lW\boldsymbol{j}|^{-1} - |2nL\boldsymbol{i} + 2lW\boldsymbol{j}|^{-1}] \tag{6}$$

An efficient algorithm to calculate G is provided by Newman [24]. From the integral equation (4), we can solve for ϕ_b on the body surface.

To calculate ϕ_b inside the fluid, we again employ Green's theorem:

$$\phi_b(\boldsymbol{r}, t) = -\frac{1}{4\pi} \iint_{S_b} \phi_b(\boldsymbol{r}', t)\boldsymbol{n} \cdot \nabla G(\boldsymbol{r} - \boldsymbol{r}')\, \mathrm{d}s' + \frac{1}{4\pi} \iint_{S_b} G(\boldsymbol{r} - \boldsymbol{r}')\boldsymbol{n} \cdot \nabla\phi_b(\boldsymbol{r}', t)\, \mathrm{d}s' \tag{7}$$

which indicates that the effect of the body can be interpreted as the combined influence of a source distribution of strength $\sigma_b = \boldsymbol{n} \cdot \nabla\phi_b(\boldsymbol{r}', t)/4\pi$ and a dipole distribution of strength $\mu_b = -\phi_b(\boldsymbol{r}', t)/4\pi$ on the body surface. The associated velocity field (including the vertical velocity on the mean free surface) can be determined by taking a spatial derivative of (7).

2. *Determination of ϕ_f*

The free-surface influence potential ϕ_f is determined from a Dirichlet boundary-value problem with its value on the mean free surface specified. At any time t, the total potential on the mean free surface $\Phi(x, y, 0, t)$ and the free-surface elevation $\zeta(x, y, t)$ are determined from time integration of the evolution equation (1). With ϕ_b and ϕ_w known, we have the Dirichlet condition on the mean free surface for ϕ_f:

$$\phi_f(\boldsymbol{r}, t) = \Phi(\boldsymbol{r}, t) - \phi_b(\boldsymbol{r}, t) - \phi_w(\boldsymbol{r}, t), \qquad \boldsymbol{r} \in \bar{S}_f \tag{8}$$

In addition, ϕ_f satisfies Laplace equation, doubly periodic boundary conditions in the horizontal plane, and the deep water condition $\nabla\phi_f \to 0$ as $z \to \infty$. This Dirichlet boundary-value problem can be resolved in a straightforward way by using a spectral approach. The solution provides the vertical derivative of ϕ_f on the mean free surface, which is necessary for integration of the evolution equation (1). It also yields $\nabla\phi_f$ anywhere inside the flow, which is required to determine the boundary condition for ϕ_b in Eq. (3) and to determine the convection velocity of the wake sheet.

3. *Determination of ϕ_w*

The wake shed from the trailing edge of the foil is modeled as an infinitely thin shear layer and is mathematically represented by a distribution of dipoles on the wake sheet. The instantaneous strength of the newly formed wake is determined by the Kutta condition, which here specifies that the strength of dipole shedding at the trailing edge μ_w equals the difference of the body influence potential ϕ_b between the upper and lower surfaces near the edge divided by 4π. This approach is a direct extension of the steady Kutta condition. In an unsteady flow, it is expected to introduce an error of $\mathcal{O}(\Delta t)$ since the body influence potential of the previous time step is used to

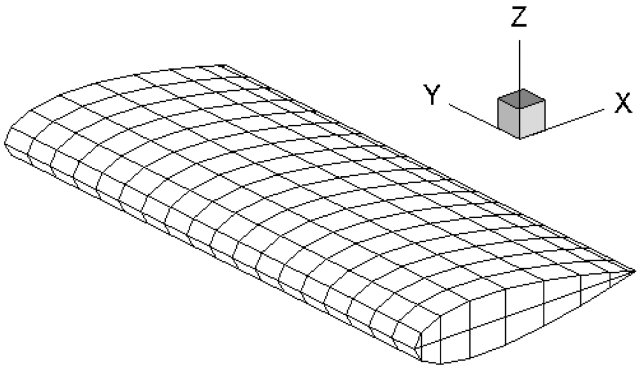

Fig. 3 Distribution of boundary elements on the foil surface.

calculate the present dipole shedding. A more accurate approach involves a Newton–Raphson iteration scheme, which enforces zero pressure difference between the upper and lower surfaces near the trailing edge [25]. This approach, however, involves the evaluation of Jacobian matrices and considerably increases the computational effort. On the other hand, through systematic convergence tests we show that our simple approach provides sufficiently accurate results with reasonably small time steps (Sec. IV.D).

Once produced, the wake is carried downstream by the fluid velocity and its strength is kept unchangeable due to the absence of dissipation. At any point $\boldsymbol{r}$ within the flow, the wake-induced potential is given by

$$\phi_w(\boldsymbol{r}, t) = \iint_{S_w} \mu_w \boldsymbol{n}' \cdot \nabla G(\boldsymbol{r} - \boldsymbol{r}')\, \mathrm{d}\boldsymbol{r}' \tag{9}$$

where s_w is the instantaneous position of the wake sheet. The associated velocity field can be obtained by taking a spatial derivative of Eq. (9).

A detailed description of the implementation of the Kutta condition and the wake sheet can be found in the literature [26] and is thus omitted here.

Table 1 Convergence of the wave drag coefficient C_d with respect to the number of body panels[a]

$N_{bs}bc$	10	20	40	80
10	1.6×10^{-2}	2.9×10^{-3}	2.6×10^{-3}	2.4×10^{-3}
20	1.1×10^{-2}	3.2×10^{-3}	2.4×10^{-3}	2.3×10^{-3}
40	1.2×10^{-2}	3.1×10^{-2}	2.5×10^{-3}	2.3×10^{-3}

[a]$C_d = F_x/\frac{1}{2}\rho scU^2$, $N_f = 128 \times 128$, $T/\Delta t = 32$, and $L = W = 100\pi c$.

Table 2 Convergence of the mean thrust coefficient C_t with respect to the number of body panels[a]

$N_{bs}bc$	10	20	40	80
10	0.097	0.178	0.182	0.181
20	0.098	0.184	0.190	0.189
40	0.099	0.187	0.194	0.193

[a]$C_t = -F_x/\frac{1}{2}\rho scU^2$, $N_f = 128 \times 128$, $T/\Delta t = 32$, and $L = W = 100\pi c$.

Table 3 Sensitivity of mean thrust coefficient C_t with respect to domain size[a]

L/c	50π	100π	200π
N_f	64×64	128×128	256×256
	0.196	0.194	0.193

[a]$N_{bs} = N_{bc} = 40$, $N_f = 128 \times 128$, $L = W$, and $T/\Delta t = 32$.

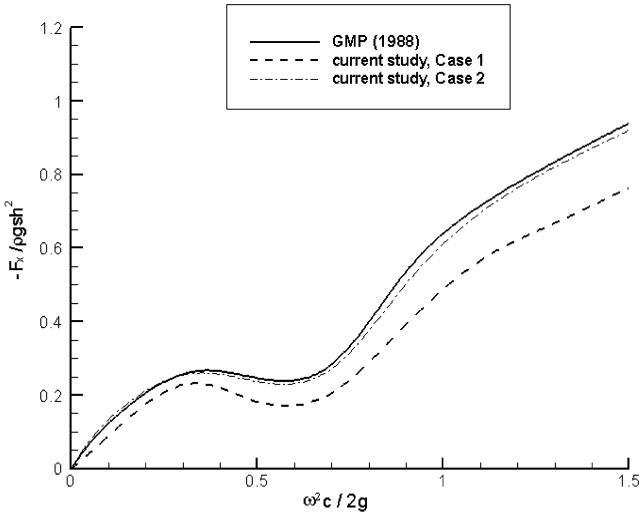

Fig. 4 Comparison of the current hybrid method with the two-dimensional linear approach by GMP. In the current result, case 1 refers to a NACA0012 foil which has a span-to-chord ratio of 5 and a heaving amplitude $h = 0.1c$. Case 2 refers to a NACA0005 foil with a span-to-chord ratio of 10 and a heaving amplitude $h = 0.025c$. The submergence is $d = 0.5c$.

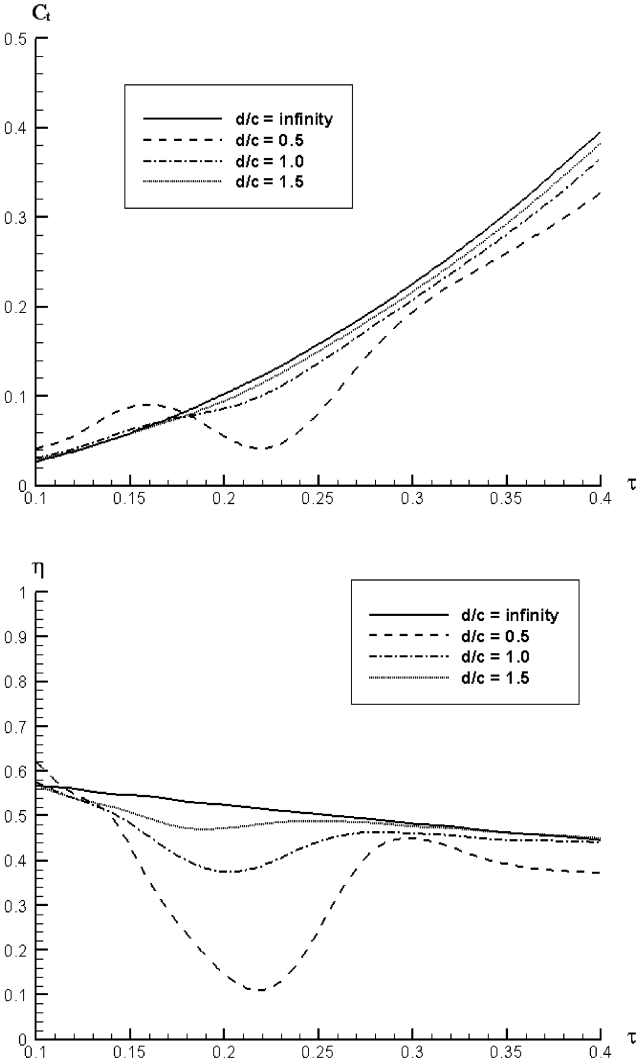

Fig. 5 The mean thrust coefficient $C_t = \bar{F}/\frac{1}{2}\rho scU^2$ and the mean propulsion efficiency η as functions of τ for a horizontal foil undergoing heaving motion. $s/c = 5$, $F_r = 0.22$, and $h/c = 0.1$.

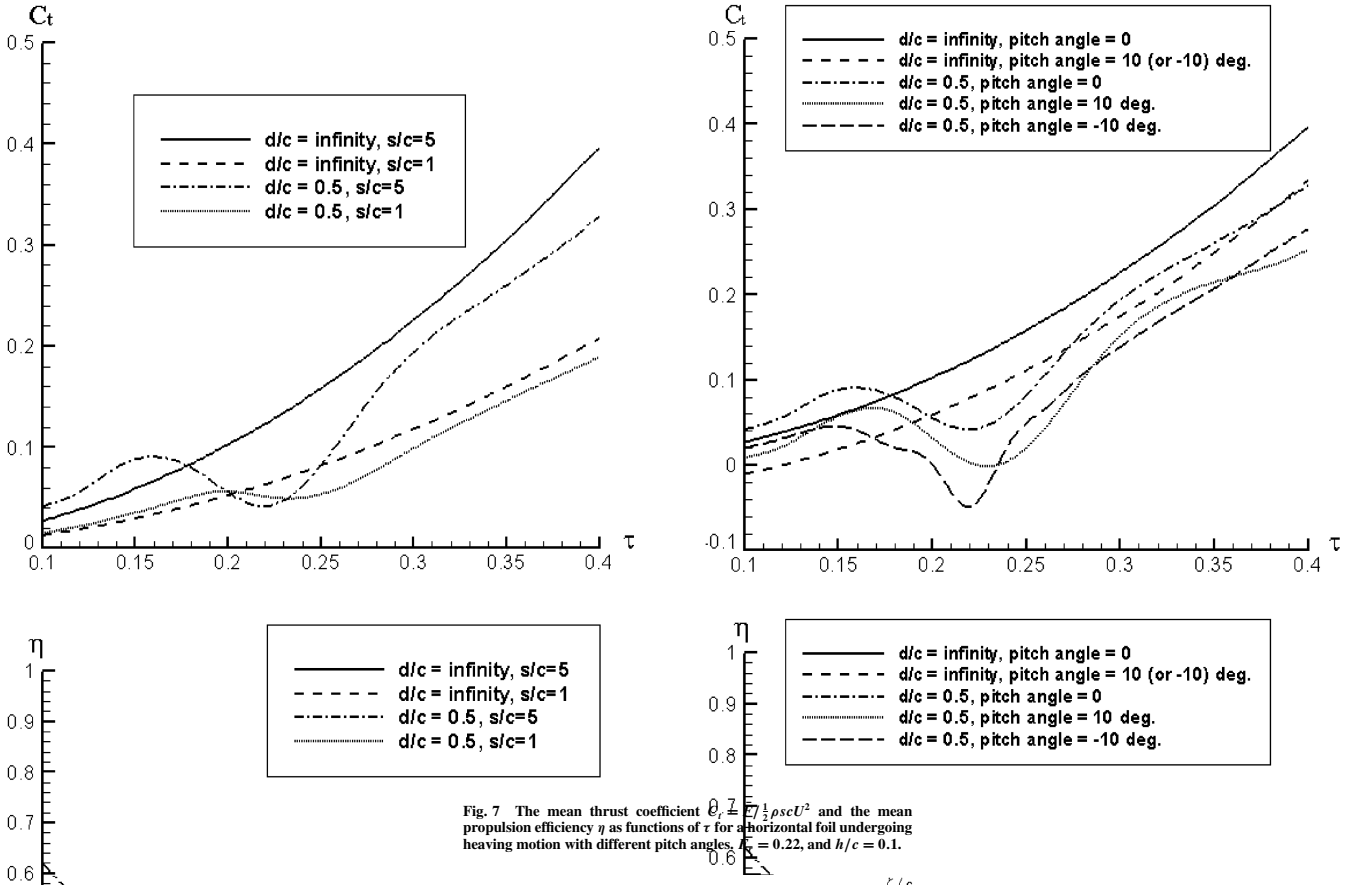

Fig. 7 The mean thrust coefficient $C_t = \bar{F}/\frac{1}{2}\rho scU^2$ and the mean propulsion efficiency η as functions of τ for a horizontal foil undergoing heaving motion with different pitch angles, $F_r = 0.22$, and $h/c = 0.1$.

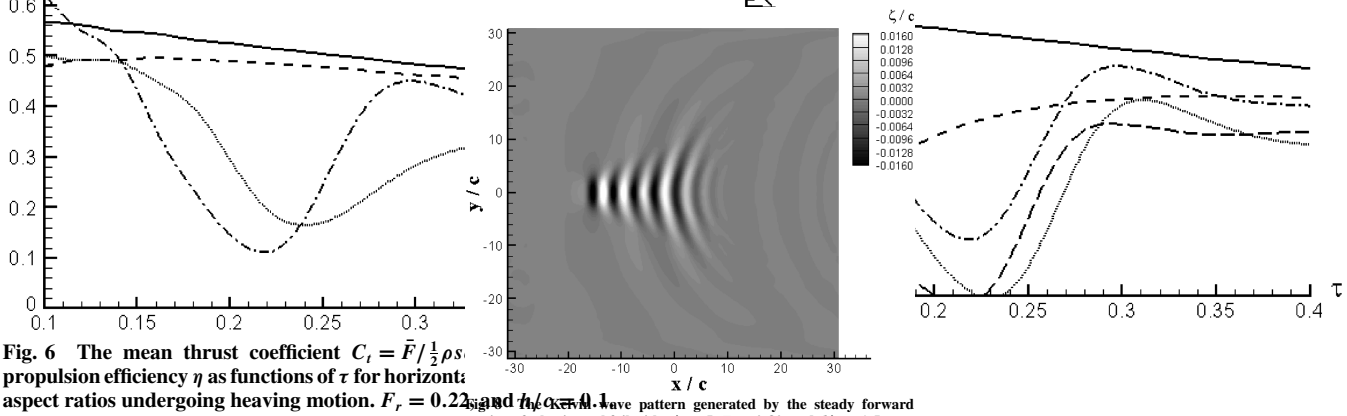

Fig. 6 The mean thrust coefficient $C_t = \bar{F}/\frac{1}{2}\rho s$ propulsion efficiency η as functions of τ for horizont aspect ratios undergoing heaving motion. $F_r = 0.22$ and $h/c = 0.1$.

Fig. 8 The wave pattern generated by the steady forward motion of a horizontal foil with $s/c = 5$, $F_r = 0.80$, and $d/c = 1.5$.

C. Hydrodynamic Force and Propulsion Efficiency

With the total velocity potential Φ given by summing up ϕ_b, ϕ_w, and ϕ_f, the hydrodynamic pressure on the body surface is readily determined from the Bernoulli equation. Integration of this pressure distribution over the foil surface gives the total hydrodynamic force $\boldsymbol{F}$ on the body:

$$\boldsymbol{F}(t) = -\rho \iint_{S_b} \left(\frac{1}{2} \nabla\Phi \cdot \nabla\Phi + \frac{\partial \Phi}{\partial t} \right) \boldsymbol{n} \, \mathrm{d}s \tag{10}$$

where ρ is the fluid density. We note that on the surface S_b of a foil undergoing unsteady motions, it is difficult to obtain $\partial\Phi/\partial t$ directly. Instead, we evaluate the material derivative $\mathrm{d}\Phi/\mathrm{d}t$. The two quantities are related by $\partial\Phi/\partial t = \mathrm{d}\Phi/\mathrm{d}t - V_b \cdot \nabla\Phi$.

The rate of energy input P to the foil required to move the body, is given by

$$P(t) = -\rho \iint_{S_b} \left(\frac{1}{2} \nabla\Phi \cdot \nabla\Phi + \frac{\partial \Phi}{\partial t} \right) \boldsymbol{V}_b \cdot \boldsymbol{n} \, \mathrm{d}s \tag{11}$$

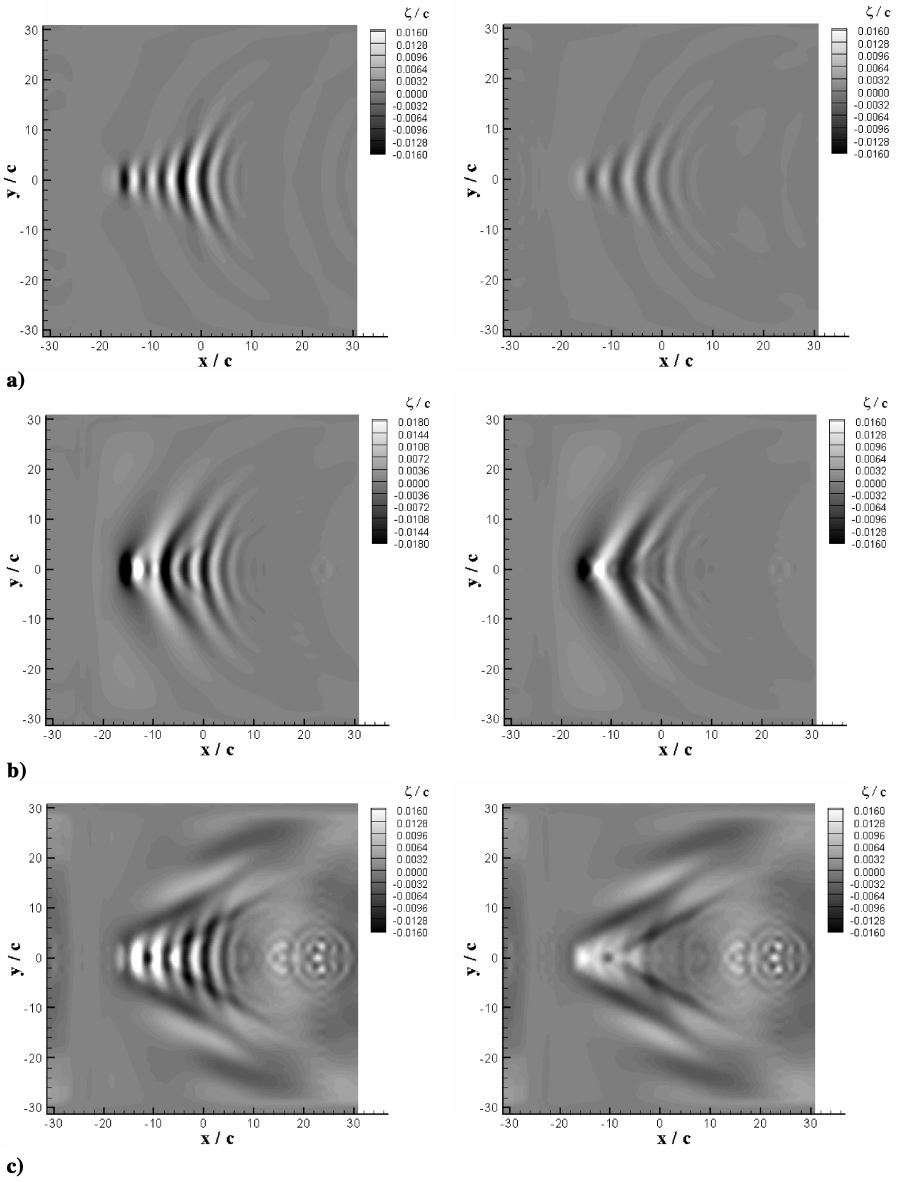

Fig. 9 Free-surface waves generated by the heaving motion of a horizontal foil with $s/c = 5$, $F_r = 0.80$, $d/c = 1.5$, and $h/c = 0.2$ at a) $\tau = 0.10$; b) $\tau = 0.25$; and c) $\tau = 0.50$. The wave fields shown are with (left) and without (right) steady Kelvin wake components.

The mean propulsive efficiency, an important measure of the foil performance, is defined as

$$\eta = U\bar{F}/\bar{P} \tag{12}$$

where U is the forward speed, $\bar{F}$ the mean hydrodynamic force in the direction of U, and $\bar{P}$ the mean energy input.

IV. Numerical Issues

A. Problem Decoupling

The coupled boundary-value problems for ϕ_b, ϕ_w, and ϕ_f need in principal to be solved simultaneously which typically requires an iteration procedure [21]. In this study, we employ a simple method to decouple the problem in the time domain. At each time step, while solving the (Neumann) boundary-value problem for ϕ_b, ϕ_w and ϕ_f are considered to be known with their values given by those at the previous time step. The same approach is applied for the determination of ϕ_w and ϕ_f. This simplification introduces an $\mathcal{O}(\Delta t)$ error. Compared with the iteration approach, which requires a small Δt to expedite convergence, our simple approach is shown to provide a satisfactory convergence with respect to the time step (Sec. IV.D) for practical applications.

B. Solution of the Boundary-Value Problems

1. Application of a Constant Panel Method for the Solution of ϕ_b

We solve the integral equation (4) for ϕ_b by a constant panel method, in which the foil surface S_b is discretized into N_b panels, S_{bj}, $j = 1, \ldots, N_b$. A sample distribution of body panels is shown in Fig. 3. The foil surface is first segmented into N_{bs} evenly distributed elements along the span. At each cross section, N_{bc} panels are applied, following a cosine distribution with high panel density near the leading and the trailing edges. In addition, N_{bc} panels are added at each end of the span to close the tips. Therefore, the total number of body panels is $N_b = (N_{bs} + 2)N_{bc}$. Over each panel, the body potential ϕ_b and its normal derivative (or, equivalently, the dipole strength μ_b and the source strength σ_b) are assumed to be constant. After applying (4) at the centroid of each panel, we obtain a linear system of N_b equations for N_b unknowns

$$\sum_{k=1}^{N_b} C_{jk}\mu_{bk} = \sum_{k=1}^{N_b} B_{jk}\sigma_{bk}, \qquad j = 1, \ldots, N_b \tag{13}$$

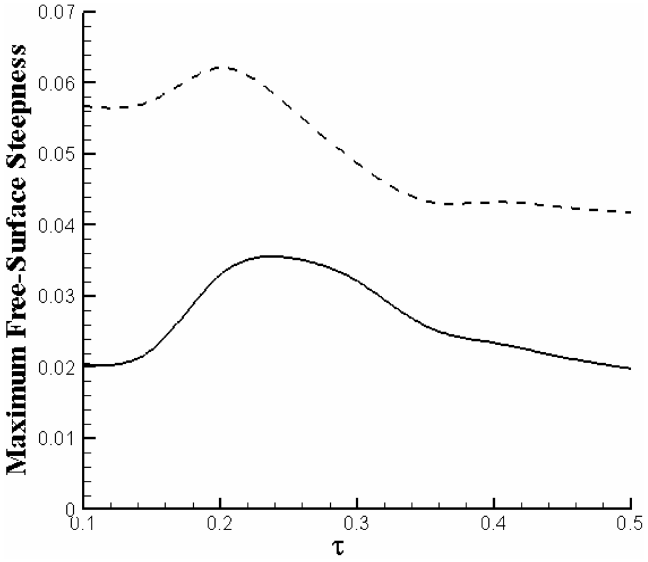

Fig. 10 Maximum local steepness of free-surface waves $\sqrt{(\partial\zeta/\partial x)^2 + (\partial\zeta/\partial y)^2}$ generated by the heaving motion of a horizontal foil with $s/c = 5$, $F_r = 0.80$, $d/c = 1.5$, and $h/c = 0.2$. Plotted are the maximum wave steepnesses of the wave field with (dashed line) and without (solid line) the steady Kelvin wave components.

where μ_{bk} and σ_{bk} are the values of μ_b and σ_b on panel S_{bk}, and

$$B_{jk} = \iint_{S_{bk}} G(\boldsymbol{r}_j - \boldsymbol{r}')\,\mathrm{d}s', \qquad C_{jk} = \iint_{S_{bk}} \boldsymbol{n}\cdot\nabla G(\boldsymbol{r}_j - \boldsymbol{r}')\,\mathrm{d}s' \quad (14)$$

where $\boldsymbol{r}_j$ is the centroid of S_{bj}. The source strength σ_{bk} in Eq. (13) is known and is given by the boundary condition (3). After Eq. (13) is solved for the unknown dipole strength, the body influence potential ϕ_b and the associated velocity anywhere in the fluid are then obtained using Eq. (7).

2. *Spectral Solution of ϕ_f*

We apply a spectral approach to solve the boundary-value problem for ϕ_f. In this approach, we express ϕ_f as a double Fourier series:

$$\phi_f(\boldsymbol{r}, t) = \sum_{j=-N_x/2+1}^{N_x/2} \sum_{k=-N_y/2+1}^{N_y/2} A_{jk}(t) e^{i\pi(jx/L + ky/W)} e^{k_{jk}z} \quad (15)$$

where $i = \sqrt{-1}$; N_x and N_y are, respectively, the number of free-surface modes employed in the x and y directions, and $k_{jk} = \pi\sqrt{(j/L)^2 + (k/W)^2}$. The potential ϕ_f in Eq. (15) satisfies all requisite conditions except for the boundary condition on the mean free surface. Upon imposing the Dirichlet boundary condition (8), the unknown modal amplitudes A_{jk} can be determined by the use of the inverse Fourier transform. Once A_{jk} is determined, ϕ_f and its spatial derivatives anywhere in the fluid domain can be evaluated easily using the Fourier transform via Eq. (15). In practice, the fast-Fourier transformation (FFT) is employed for these purposes. The requisite computational effort is $\mathcal{O}(N_f \log N_f)$, where $N_f = N_x N_y$ is the total number of spectral modes used.

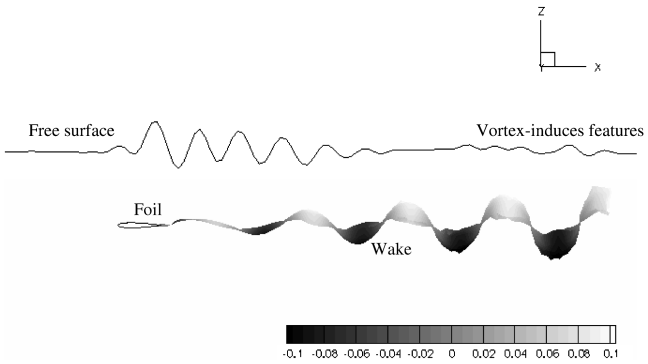

Fig. 11 Wake shedding and free-surface signatures (within the symmetric plane) generated by a foil undergoing heaving and translation ($s/c = 5$, $F_r = 0.80$, $\tau = 0.50$, $h/c = 0.2$, and $d/c = 1.5$). The contour shows the strength of the dipole distribution in the wake, normalized by Uc. Note that the size of the foil and the amplitude of the wave are exaggerated for better illustration.

C. Time Integration

At each time step t, we first solve the boundary-value problems for ϕ_b and ϕ_f, and determine the strength of the newly created wake from the Kutta condition at the trailing edge of the foil. With the velocity field determined, the locations of the existent wake panels are updated using a forward Newtonian scheme. We then integrate the evolution equation (1) forward in time based on the 4th-order Runge–Katta scheme to obtain the updated free-surface elevation and potential.

We note that a discretely distributed vorticity as used in the current model is susceptible to instabilities. To stabilize the computation, it is necessary to introduce a desingularization algorithm [27]. According to this algorithm, we assign a finite core radius δ to each (body or wake) panel of dipole distribution. The induced velocity at any point by this panel will then be evaluated through the desingularized Biot–Savart law:

$$\boldsymbol{V}(x) = \frac{\Gamma}{4\pi}\oint \frac{\boldsymbol{s}\times\boldsymbol{r}}{r^3 + \delta^3}\,\mathrm{d}l \quad (16)$$

where Γ is the circulation of the vortex ring around the sides of the panel which is equivalent to the uniform normal dipole distribution inside the panel, $\boldsymbol{s}$ is the tangent vector of the panel, $\boldsymbol{r}$ is the vector from the integration element to the field point, $r = |\boldsymbol{r}|$, and the path of integration is along the four sides of the panel. The inclusion of the desingularization factor effectively prevents the ill-posed dynamic problem associated with zero-thickness shear layers and stabilizes wake evolution. By systematic convergence tests, it has been demonstrated that within a reasonable range of δ, the hydrodynamic forces on the body are not sensitive to the value of δ [22].

D. Validations

The validity and accuracy of both the panel method and the spectral algorithm have been extensively examined and demonstrated for problems without coupling of foil, wake, and free surface [22,28,29]. We present here convergence tests and comparisons to existing numerical results to validate the efficacy of the present hybrid method for the coupled foil-wake-free surface problem.

1. *Convergence Tests*

To demonstrate the convergence of the hybrid scheme, we first choose as a sample case, the steady translation of a foil with its span parallel to the free surface. At each cross section along the span, the foil has a NACA0012 profile with maximum thickness to chord ratio 0.12 and zero camber. The span (s) to chord (c) ratio is 5. The submergence d, defined as the distance from the mean free surface to the mean position of the chord (Fig. 1), is $0.5c$, $\tau = 0.30$, and the Froude number is $F_r = 0.22$. The foil also has a pitch angle of 10 deg, with the pitch axis located at $1/3$ chord from the leading edge.

Table 1 shows the wave drag, which is the difference between the drag on the foil moving near the free surface and that on one moving in infinite fluid, as a function of N_{bs}, the number of body panels in span, and N_{bc}, the number of panels in chord. The number of free-surface spectral modes is $N_f = 128 \times 128$, and the time step $\Delta t = 0.65\ U/g$. Linear convergence with respect to both N_{bs} and N_{bc} is observed.

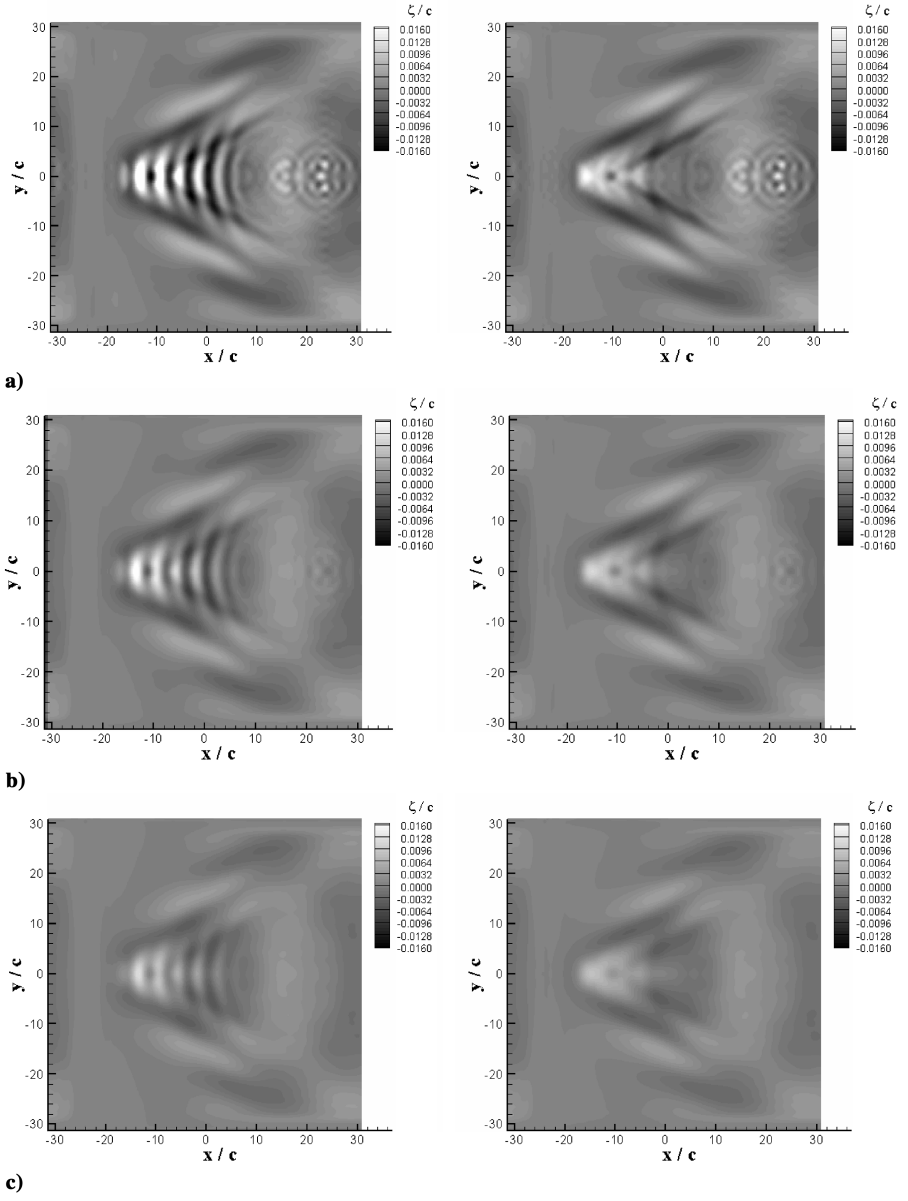

Fig. 12 Free-surface signature generated by the heaving motion of a horizontal foil with $s/c = 5$, $F_r = 0.80$, $\tau = 0.50$, $h/c = 0.2$, and a) $d/c = 1.5$; b) $d/c = 2.0$; and c) $d/c = 2.5$. The wave fields shown are with (left) or without (right) steady Kelvin wake components.

We further study the convergence of our scheme in an unsteady problem by considering the above mentioned foil undergoing a translation and a periodic heaving motion. The pitch angle is fixed as zero, whereas the heaving amplitude is $h = 0.1c$.

Table 2 shows the mean thrust coefficient $C_t = -F_x/\frac{1}{2}\rho scU^2$ as a function of N_{bs} and N_{bc}. The number of free-surface spectral modes is fixed as $N_f = 128 \times 128$, and the time step $\Delta t = T/32$, where T is the period of heave motion. Although the method is relatively low order with respect to body panel size, for the reasonably large number of body panels in Table 1, the result converges to around 2%. As expected, the convergence with respect to the number of free-surface modes (for fixed number of modes and time step) is even better. Indeed, the exponential convergence of the lift coefficient with increasing N_f ($N_{bs} = N_{bc} = 40$, $T/\Delta t = 32$, $L = W = 100\pi c$) is obtained as follows: 0.190 for N_f of 64×64, 0.194 for N_f of 128×128, and 0.194 for N_f of 256×256.

The mean thrust coefficient can be shown as a function of time step. The mean thrust coefficient C_t converges as follows with respect to Δt ($N_{bs} = N_{bc} = 40$, $N_f = 128 \times 128$, $L = W = 100\pi c$): 0.266 for $T/\Delta t$ of 8, 0.205 for $T/\Delta t$ of 16, 0.194 for $T/\Delta t$ of 32, and 0.190 for $T/\Delta t$ of 64. It is clear that despite the fact that the time integration we use is a first-order explicit scheme, and no iterations are employed in solving the coupled problems, the result still converges to around 3%.

Convergence tests are also performed to examine the influence of the size of the computational domain, as displayed in Table 3. It is seen that the mean thrust coefficient is not sensitive to changes in L or W. Similarly, we confirm that when the desingularization factor is within a reasonably large range ($0.01c \leq \delta \leq 0.1c$), it has virtually no effect on the result.

Based on extensive convergence tests such as these, for all our subsequent numerical results, the following computational parameters are used: $N_{bs} = N_{bc} = 40$, $N_f = 128 \times 128$, $L = W = 100\pi c$, $\delta = 0.05c$, and $\Delta t = T/32$.

2. *Comparison with Existing Results*

As a further validation of the present method, we compare our results with those of Grue et al. [19] (hereafter referred to as GMP) who obtained an accurate numerical result for the periodic heaving of a horizontal foil under the free surface. In GMP, the problem is two dimensional, and the foil boundary condition is satisfied at its mean position. We note that our model includes several effects not present in GMP: three dimensionality, finite foil thickness, and nonlinear

body/vortex motion. To address these differences, we study two cases: case 1 refers to a NACA0012 foil with a span-to-chord ratio of 5 and a heaving amplitude $h = 0.1c$, and case 2 refers to a NACA0005 foil with a span-to-chord ratio of 10 and a heaving amplitude $h = 0.025c$. It is clear that by minimizing the effects of the finite aspect ratio, the foil thickness, and the nonlinear motion, case 2 is much closer to GMP.

Figure 4 plots the normalized thrust of the foil as a function of the oscillating frequency. The Froude number $F_r = 0.18$. The comparison between GMP and the present results in case 2 is overall satisfactory while the differences between GMP and out results in case 1 can be attributed to the above mentioned differences. Figure 4 shows that, at small frequencies, the presence of a free surface increases the thrust, but the effect is reversed when the frequency is increased. The influence of the free surface is most significant for the parameter $\omega^2 g/2c$ larger than 0.3.

V. Numerical Results

In forward speed (U) oscillatory problems (frequency ω) involving the free surface (under gravity g), it is well known that an important dimensionless parameter governing the dynamics is $\tau \equiv U\omega/g$ [30]. Of special interest is the behavior of the problem near the critical value $\tau = \tau_c \equiv 0.25$ [31]. In two-dimensional oscillatory problems with forward speed, four propagating waves, two going upstream and two downstream, are generated for $\tau < \tau_c$ (subcritical), while the two upstream waves disappear for $\tau > \tau_c$. At $\tau = \tau_c$, the group velocity of radiated waves matches the forward speed of the body, and the linearized problem is singular for a point source. Although the problem is regularized for bodies with a finite volume [32] or in the presence of shed wakes [33], the strong behavior and dependence on τ near the critical value is still generally present. In the following, we consider the advancing oscillatory foil problem over a range of values of τ with special interest in the dynamic behavior near $\tau = \tau_c$.

A. Heaving Motion of a Horizontal Foil

For a horizontal foil undergoing heaving motion (the pitch angle is kept as zero), Fig. 5 plots the mean thrust coefficient C_t and the propulsion efficiency η as functions of τ at different submergences. The Froude number is $F_r = 0.22$. The presence of free surface increases (decreases) the thrust for $\tau \lessapprox 0.18$ ($\tau \gtrapprox 0.18$). Though the thrust may be increased, the propulsion efficiency is generally decreased in the presence of free surface except for the case of very small submergence and small values of τ ($d/c = 0.5$ and $\tau \lessapprox 0.12$) in which the efficiency may be increased. Such an effect due to free surface is much more profound in the region around the critical value $\tau = \tau_c \equiv 0.25$. In particular, the efficiency can be reduced by as large as ~80% for the case of shallow submergence ($d/c = 0.5$). We repeated these calculations for different Froude numbers and found that the results are qualitatively similar to those in Fig. 5. Thus, in terms of quantities such as thrust and efficiency, it is predominantly τ, rather than F_r, that controls the dynamics of a foil operating near the free surface. We also note that with oscillations, the thrust on the foil is at least 1 order larger than the wave drag (Table 1).

Figure 6 displays the effect of the aspect ratio on the dynamic property of a submerged foil for $d/c = \infty$ and $d/c = 0.5$. Two different aspect ratios, $s/c = 5$ and $s/c = 1$, are considered. The results indicate that both thrust coefficient and propulsion efficiency have a strong dependence on the aspect ratio of the foil. In the absence of free surface, both thrust and propulsion efficiency are larger for the foil with larger aspect ratio, owing to the existence of induced drag. This implies that the presence of the three-dimensionality effect reduces the foil performance. When the foil operates near the free surface, the performance of the foil is significantly deteriorated, especially in the neighborhood of $\tau = \tau_c$. The dependence on the aspect ratio of the foil is more complex. In particular, in contract to the case without the free-surface influence, the foil with the smaller aspect ratio may outperform that with a larger aspect ratio.

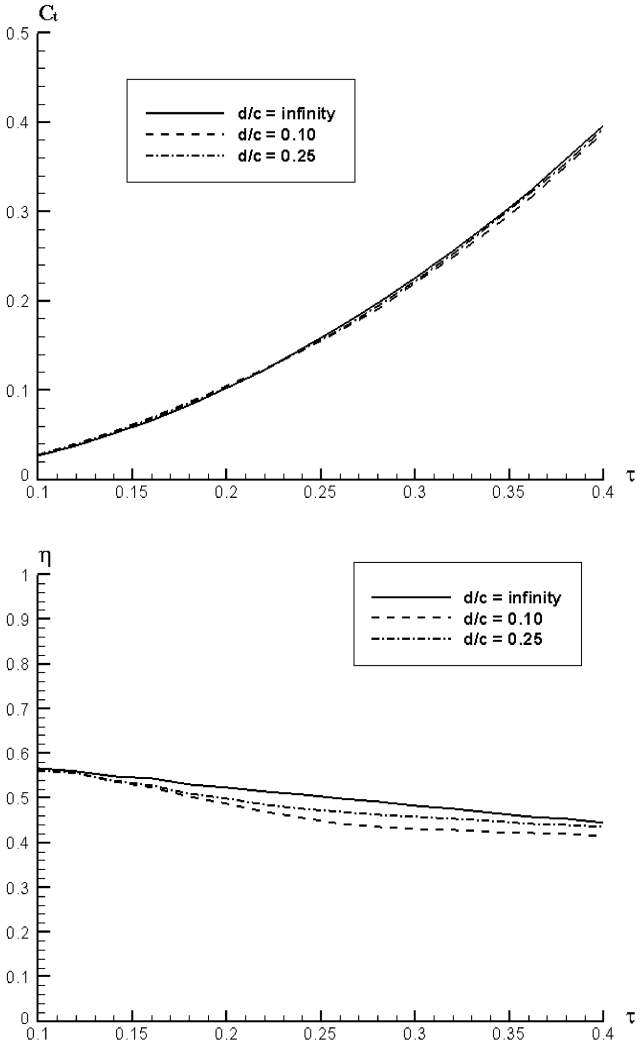

Fig. 13 The mean thrust coefficient $C_t = \bar{F}/\frac{1}{2}\rho scU^2$ and the mean propulsion efficiency η as functions of τ for a vertical foil undergoing swaying motion. $F_r = 0.22$, and $h/c = 0.1$.

The effect of pitch angles on the overall performance of the foil is shown in Fig. 7. Two pitch angles, 10 deg (bow-up) and −10 deg (bow-down) are considered. The pitch axis is located at a point that is 1/3 chord from the leading edge. In all the cases, the pitch angle reduces both the thrust and the efficiency. Indeed, without the free surface negative thrust is observed in the bow-up case when τ is small ($\tau \lessapprox 0.12$). With the presence of a free surface, in the bow-down case when τ is close to the critical value the thrust also becomes negative.

The free-surface signature of a translating and heaving foil is composed of three contributions: the steady Kelvin wave pattern associated with the steady forward motion consisting of the transverse and diverging wave systems; the unsteady wave pattern generated by the oscillatory motion; and the waves generated by vortices in the wake. In the absence of oscillatory motions, the wave disturbance shows the characteristics of a Kelvin wave pattern, with the waves confined within a wedge of angle 35.5 deg (Fig. 8). At this particular value of Froude number ($F_r = 0.80$) and submergence ($d/c = 1.5$), the wave field is composed mostly of the transverse waves propagating along the track of the body.

Figure 9 shows combined features of the free surface due to forward speed and oscillation of the foil for different values of τ, plotted with and without the Kelvin wake component. In all these cases, the heaving motion amplitude is $h/c = 0.2$. At the subcritical value of $\tau = 0.10$ (Fig. 9a), the unsteady wave pattern appears much weaker than the Kelvin pattern. At the critical value $\tau = 0.25$ (Fig. 9b), the wave field is dominated by the unsteady waves, demonstrating a distinctive pattern different from the Kelvin wake.

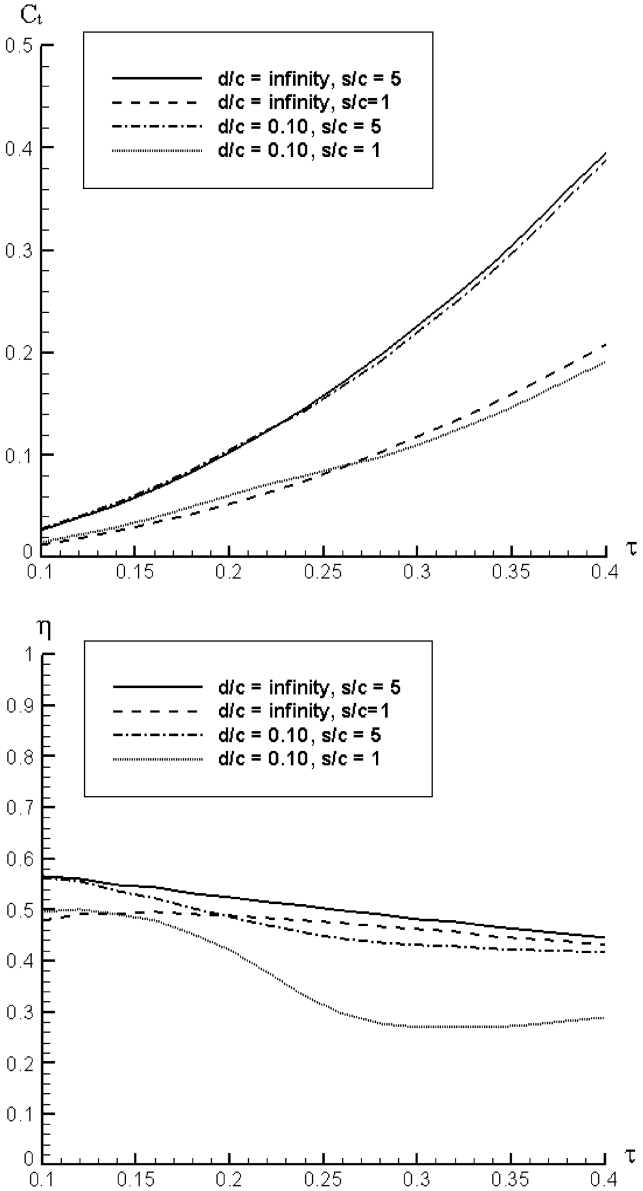

Fig. 14 The mean thrust coefficient $C_t = \bar{F}/\frac{1}{2}\rho scU^2$ and the mean propulsion efficiency η as functions of τ for vertical foils with different aspect ratios undergoing swaying motion. $F_r = 0.22$, and $h/c = 0.1$.

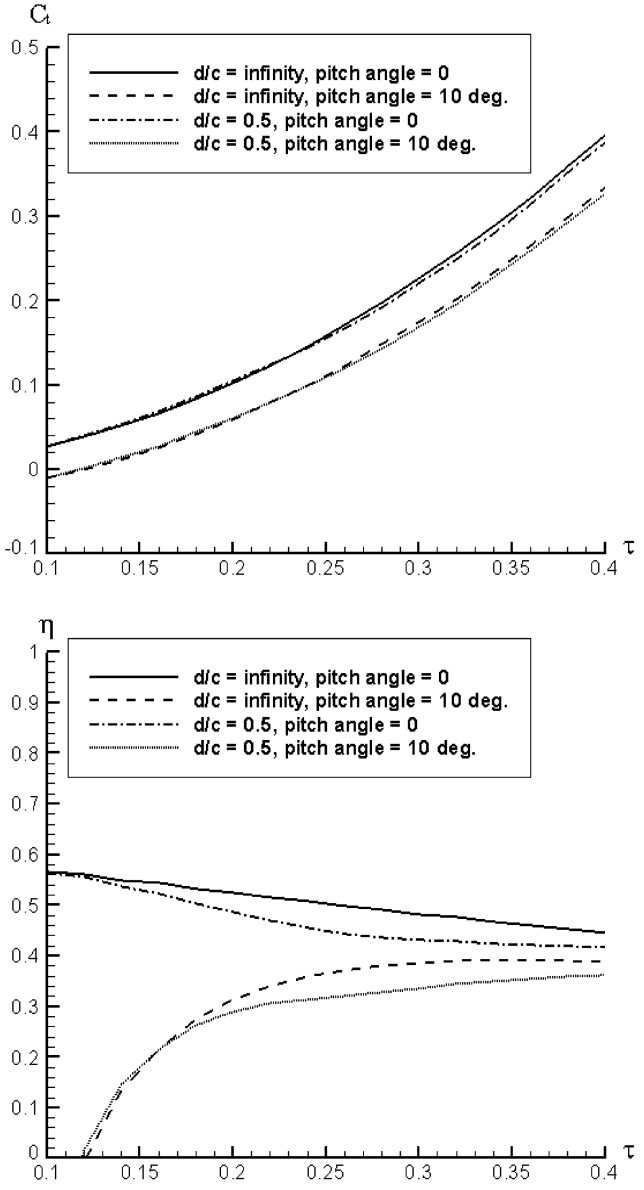

Fig. 15 The mean thrust coefficient $C_t = \bar{F}/\frac{1}{2}\rho scU^2$ and the mean propulsion efficiency η as functions of τ for a vertical foil with different pitch angles undergoing swaying motion. $F_r = 0.22$, and $h/c = 0.1$.

At the supercritical value of $\tau = 0.50$, the unsteady waves become less pronounced and the Kelvin-like wave field reappears (Fig. 9c). In addition, a sequence of ring-shaped ripples on the track due to the underlying vortex wake is shown. The effect of τ on the free-surface wave steepness is shown in Fig. 10, which demonstrates that the largest wave steepness is achieved in the vicinity of $\tau = \tau_c$.

The key features in the interaction of the vortex wake with the free surface are depicted in Fig. 11. The shed wake, which has initially a periodic vorticity strength, evolves under self-induction into a characteristic meandering sheet with vorticity concentrated near the peaks and troughs. Eventually, the sheet curls up and evolves into a sequence of individual counter-rotating vortices. When the mean hydrodynamic force on the foil is a thrust, the wake takes the form of the reverse Kármán vortex street [34], in which the vortices near the peaks of the sheet are counterclockwise (corresponding to positive dipole concentrations in Fig. 11), while those near the troughs are clockwise (negative dipole concentrations). When the foil experiences (mean) drag force, the wake resembles the classical Kármán street in which the rotational directions of the vortices are reversed. In both cases, the wake contains two arrays of vortices, one of them close to the free surface and the other far below. When the vortices in the upper row approach the free surface, they induce the characteristic sequence of ringlike wave features observed in Fig. 9c. The distance between two neighboring rings is determined by the Strouhal number S_t, and is expressed as $\frac{2h}{S_t} = 2\pi cF_r^2/\tau$. Based on this estimation, this distance in Figs. 9a–9c is $40c$, $16c$, and $8c$, respectively. It is clear that the vortex-induced features in Fig. 9a are out of the computational domain.

Figure 12 shows the dependence of the free-surface wave pattern on the submergence of the foil. At all submergences we study, both the steady Kelvin pattern and the unsteady wave contribute to the overall free-surface signature, although both of them decay with submergence. Indeed, the total wave fields at different submergences resemble each other, except for the ringlike features caused by the vorticity wake, which disappear in deep submergence (Fig. 12c), indicating that they decay with the body submergence at a faster rate.

B. Swaying Motion of a Vertical Foil

Unlike the horizontal-foil case, which approaches a two-dimensional problem in the limit of long span, the problem of a vertical foil in sway motion cannot be simplified as a two-dimensional problem near the surface. In the following, we use our three-dimensional hybrid method to investigate this problem.

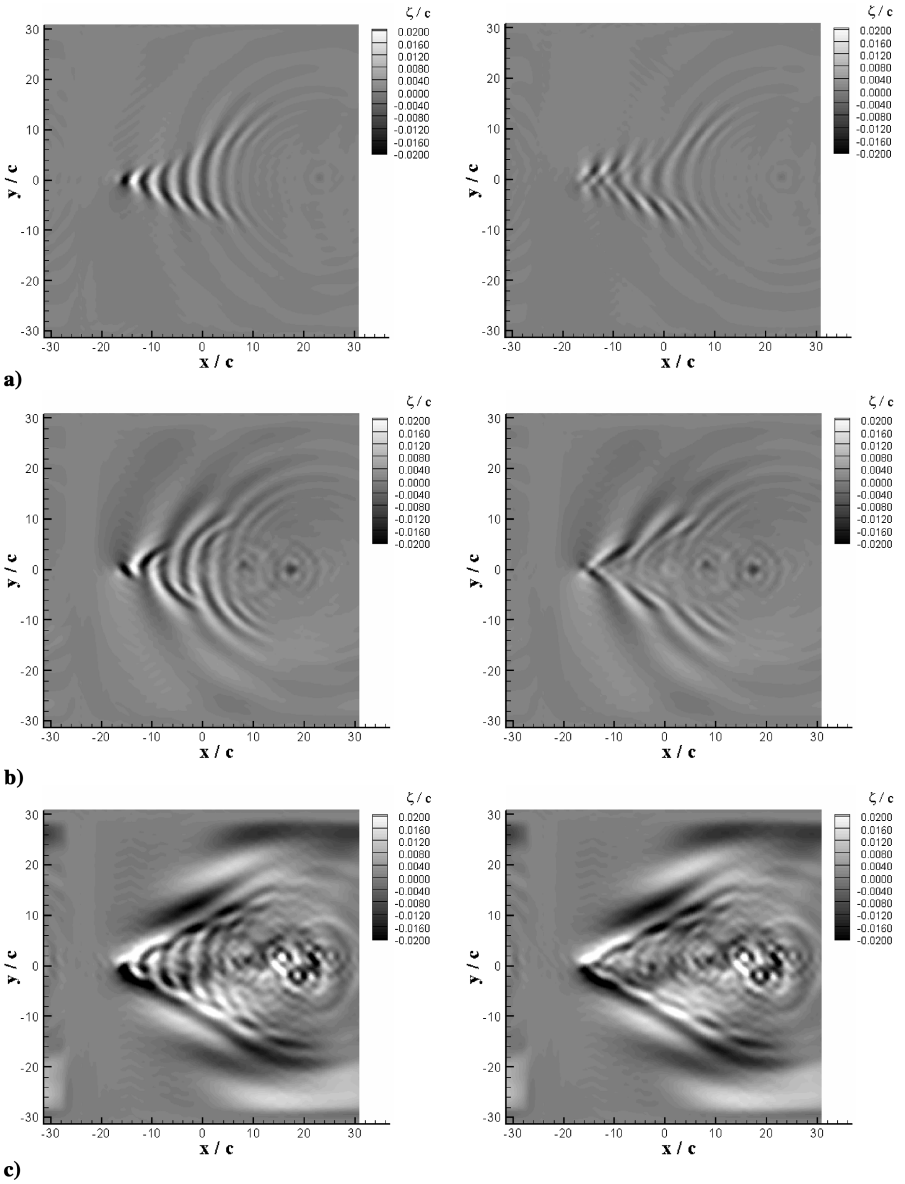

Fig. 16 Free-surface waves generated by the heaving motion of a vertical foil with $s/c = 5$, $F_r = 0.80$, $d/c = 0.5$, and $h/c = 0.25$ at a) $\tau = 0.10$ b) $\tau = 0.25$, and c) $\tau = 0.50$. The wave fields shown are with (left) or without (right) steady Kelvin wake components.

In Fig. 13, we plot the mean thrust force and the propulsion efficiency on a vertical foil undergoing swaying motions at $F_r = 0.22$. The submergence d is defined to be the distance from the undisturbed free surface to the top tip of the foil. The mean thrust coefficient generally increases with τ whereas the propulsion coefficient decreases with τ. Compared with the horizontal-foil case, the influence of the free surface is not as significant, especially for the thrust. This is because a large portion of the foil is deeply submerged even for relatively small d. In addition, the large performance reduction near the critical τ is not observed in the mean thrust or the propulsion efficiency. This can be explained by the fact that the dominant waves radiated from the foil in this case are in the direction perpendicular to the track, while the wave components propagating along the track, which would be accumulated around the foil at the critical value of τ, are relatively small.

Figure 14 shows the effect of aspect ratio on the dynamic property of a vertical. A large aspect ratio foil with $s/c = 5$ and a small aspect ratio foil with $s/c = 1$ are considered. In the small aspect ratio case, in addition to the reduction of thrust and propulsion efficiency due to the induced drag, a much larger free-surface effect is observed. For the large aspect ratio foil, the maximum changes caused by the free surface in the thrust and the efficiency are about 3% and 11%, respectively. In contrast, for the small aspect ratio foil the maximum thrust reduction is about 8%, while the propulsion efficiency is decreased by 40%. This is explained by the fact that the average submergence of the foil is reduced by decreasing the aspect ratio.

In Fig. 15, we plot the mean thrust and propulsion efficiency of a vertical foil with different pitch angles. Similar to the horizontal-foil case, when τ is small a pitch angle of 10 deg significantly reduces the thrust and efficiency, leading to negative thrust as $\tau < 0.12$. This effect becomes less pronounced as τ is increased.

This insensitivity to the critical value of τ is also shown in the free-surface wave patterns (Fig. 16) and the maximum local steepness of the generated waves (Fig. 17). The unsteady waves are nonsymmetrical with respect to the track of the foil. As τ increases, the wave number and amplitude of the unsteady waves increase accordingly, while the abrupt rise of the amplitude of the unsteady waves in the region near $\tau = \tau_c$ is not observed. The vortex-induced waves appear as well and generally become stronger with larger values of τ. These vortex-induced waves appear on ringlike shapes. Their locations correspond to the position of the underlying vortices in a Kármán (or reverse Kármán) vortex street and are therefore away from the centerline and exhibit the characteristic meandering pattern of the vortex street. The distance between two neighboring rings in the x direction is estimated to be $\frac{h}{S_t} = \pi c F_r^2/\tau$, which is estimated to be $20c$, $8c$, and $4c$ for the cases in Figs. 16a–16c, respectively.

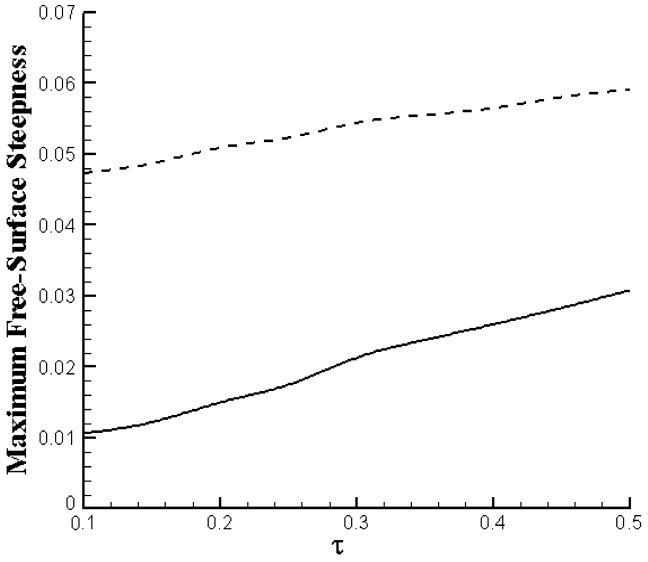

Fig. 17 Maximum local steepness of free-surface waves $\sqrt{(\partial\zeta/\partial x)^2 + (\partial\zeta/\partial y)^2}$ generated by the swaying motion of a vertical foil with $s/c = 5$, $F_r = 0.80$, $d/c = 0.5$, and $h/c = 0.25$. Plotted are the maximum steepnesses of the wave field with (dashed line) and without (solid line) the steady Kelvin wave components.

VI. Conclusions

Applying a hybrid numerical scheme combining a boundary-element method and a spectral method, we study the problem of heaving/swaying horizontal/vertical foils near the free surface at varying forward speeds, submergences, and oscillating frequencies. On one hand, by using a boundary-element method with a shear-layer representation of the vorticity wakes, the algorithm allows for arbitrary geometry, nonlinear body motion, and vorticity shedding. On the other hand, the spectral method provides an accurate representation of the free-surface waves in both near and far fields.

In the horizontal-foil case, the dynamic behavior is strongly determined by the parameter τ with the most significant effect occurring around $\tau = \tau_c \equiv 0.25$. Except for very small values of τ at very shallow submergence, the presence of the free surface decreases both mean thrust coefficient and propulsion efficiency. Away from the critical τ, the presence of the free surface increases the thrust and efficiency at low frequencies and decreases them at high frequencies. In certain cases, the thrust is increased while the efficiency is decreased (e.g., in Fig. 5 when $d/c = 0.5$ and $0.12 < \tau < 0.18$). The opposite case is also recorded (e.g., in the same figure when $d/c = 1.5$ and $\tau > 0.35$). One of the physical mechanisms that may have caused such a complicate behavior is the thrust (or drag) caused by the unsteady wave generation. For example, in a two-dimensional case, at subcritical τ four propagating waves are generated by a translating body undergoing oscillations. Three of these waves propagate in the same direction as the body translation and cause drag, while the fourth wave propagates in the opposite direction and generates thrust. The overall wave thrust/drag is thus determined by the magnitudes of these propagating waves. Another possible mechanism is the interaction between free-surface waves and the vorticity wake. At certain parameters, the energy of the bow wave may be absorbed by the trailing edge in the process of wake generation so that the overall efficiency may be increased. Further investigations are needed to illustrate the exact mechanism.

On the free surface, in addition to the conventional Kelvin wave pattern associated with the translation of the foil, two other waves systems are also found. One is the unsteady wave generated by the oscillation motion, which is most pronounced near the critical value of τ. The other is the wave pattern induced by the vortices shed from the foil, which concentrates around the track of the foil and decays rapidly as submergence is increased. For small submergence, each vortex in the wake generates a distinctive ringlike wave pattern.

The surface signature of the swaying vertical foil is distinct from that of the horizontal case in that the unsteady waves propagate mostly in the transverse direction. Consequently there is no significant accumulation of radiated waves occurring near the critical τ, and neither the radiated wave fields nor the hydrodynamic loads display strong sensitivity at τ_c. In addition, the vortex-induced surface patterns are now located off the centerline with the centers of the ringlike patterns displaying a meandering feature.

References

[1] Lighthill, M. J., "Aquatic Animal Propulsion of High Hydrodynamical Efficiency," *Journal of Fluid Mechanics*, Vol. 44, 1970, pp. 265–301.
[2] Triantafyllou, M. S., and Triantafyllou, G. S., "An Efficient Swimming Machine," *Scientific American*, Vol. 272, 1995, pp. 64–70.
[3] Anderson, J. M., Streitlien, K., Barret, D. S., and Triantafyllou, M. S., "Oscillating Foils for High Propulsive Efficiency," *Journal of Fluid Mechanics*, Vol. 360, 1998, pp. 41–72.
[4] Read, D. A., "Oscillating Foils for Propulsion and Maneuvering of Ships and Underwater Vehicles," M.S. Thesis, MIT, 2000.
[5] Campbell, M., "Concept Development of an Oscillating Tidal Power Generator," *Proceedings of ASME Fluids Engineering Division Summer Meeting*, American Society of Mechanical Engineers, Fairfield, NJ, July 2002.
[6] Koochesfahani, M. M., "Vortical Patterns in the Wake of an Oscillating Airfoil," *AIAA Journal*, Vol. 27, 1988, pp. 1200–1205.
[7] Theodorsen, T., "General Theory of Aerodynamic Instability and the Mechanism of Flutter," National Advisory Committee for Aeronautics, Rept. 496, 1935.
[8] Triantafyllou, G. S., Triantafyllou, M. S., and Grosenbaugh, M. A., "Optimal Thrust Development in Oscillating Foils with Application to Fish Propulsion," *Journal of Fluids and Structures*, Vol. 7, 1993, pp. 205–224.
[9] Liu, H., and Kawachi, K., "A Numerical Study of Insect Flight," *Journal of Computational Physics*, Vol. 146, 1998, pp. 124–56.
[10] Wang, Z. J., "Vortex Shedding and Frequency Selection in Flapping Flight," *Journal of Fluid Mechanics*, Vol. 410, 2000, pp. 323–341.
[11] Rammamurti, R., and Sandberg, W. C., "A Three-Dimensional Computational Study of the Aerodynamic Mechanisms of Insect Flight," *Journal of Experimental Biology*, Vol. 205, 2002, pp. 1507–1518.
[12] Plotkin, A., "The Thin-Hydrofoil Thickness Problem Including Leading-Edge Corrections," *Journal of Ship Research*, Vol. 19, No. 2, 1975, pp. 122–129.
[13] Giesing, J. P., and Smith, A. M. O., "Potential Flow About Two-Dimensional Hydrofoils," *Journal of Fluid Mechanics*, Vol. 1, 1967, pp. 113–129.
[14] Yeung, R. W., and Bouger, Y. C., "A Hybrid Integral-Equation Method for Steady Two-Dimensional Ship Waves," *International Journal for Numerical Methods in Engineering*, Vol. 14, 1979, pp. 317–336.
[15] Salvesen, N., "On Higher-Order Wave Theory for Submerged Two-Dimensional Bodies," *Journal of Fluid Mechanics*, Vol. 38, 1969, pp. 415–432.
[16] Kennell, C., and Plotkin, A., "A Second-Order Theory for the Potential Flow About Thin Hydrofoils," *Journal of Ship Research*, Vol. 28, No. 1, 1984, pp. 55–64.
[17] Tsai, W. T., and Yue, D. K. P., "Interactions Between a Free-Surface and a Vortex Shed in the Wake of a Surface-Piercing Plate," *Journal of Fluid Mechanics*, Vol. 257, 1993, pp. 691–721.
[18] Chen, T., and Chwang, A. T., "Trailing Vortices in a Fee-Surface Flow," *Physics of Fluids*, Vol. 14, No. 2, 2002, pp. 827–838.
[19] Grue, J., Mo, A., and Palm, E., "Propulsion of a Foil Moving in Water Waves," *Journal of Fluid Mechanics*, Vol. 186, 1988, pp. 393–417.
[20] Isshiki, H., Murakami, M., and Terao, Y., "Utilization of Wave Energy into Propulsion of Ships—Wave Devouring Propulsion," *15th Symposium On Naval Hydrodynamics*, 1984, pp. 539–552.
[21] Bal, S., Kinnas, S. A., and Lee, H., "Numerical Analysis of 2-D and 3-D Cavitating Hydrofoils Under s Free Surface," *Journal of Ship Research*, Vol. 45, No. 1, 2001, pp. 34–49.
[22] Zhu, Q., Wolfgang, M., Yue, D. K. P., and Triantafyllou, M. S., "Three-Dimensional Flow Structures and Vorticity Control in Fish-Like Swimming," *Journal of Fluid Mechanics*, Vol. 468, 2002, pp. 1–28.
[23] Cao, Y., "Computations of Nonlinear Gravity Waves by a Desingularized Boundary Integral Method," Ph.D. Thesis, The University of Michigan, 1991.
[24] Newman, J. N., "The Green Function for Potential Flow in a Rectangular Channel," *Journal of Engineering Mathematics*, Vol. 26, 1992, pp. 51–59.

[25] Kinnas, S. A., and Hsin, C.-Y., "A Boundary Element Method for the Analysis of the Unsteady Flow Around Extreme Propeller Geometries," *AIAA Journal*, Vol. 30, 1992, pp. 688–696.
[26] Katz, J., and Plotkin, A., *Low-Speed Aerodynamics: from Wing Theory to Panel Methods*, McGraw–Hill, New York, 1991.
[27] Krasny, R., "Desingularization of Periodic Vortex Sheet Roll-Up," *Journal of Computational Physics*, Vol. 65, 1986, pp. 292–313.
[28] Dommermuth, D. G., and Yue, D. K. P., "A High-Order Spectral Method for the Study of Nonlinear Gravity Waves," *Journal of Fluid Mechanics*, Vol. 184, 1987, pp. 267–288.
[29] Liu, Y., Dommermuth, D. G., and Yue, D. K. P., "A High-Order Spectral Method for Nonlinear Wave-Body Interactions," *Journal of Fluid Mechanics*, Vol. 245, 1992, pp. 115–136.
[30] Haskind, M. D., "On Wave Motion of a Heavy Fluid," *Prikladnaya Matematika i Mekhanika*, Vol. 18, 1954, pp. 15–26.
[31] Wehausen, J. V., and Laitone, E. V., *Surface Waves*, in Handbuch der Physik, Springer, New York, 1960, pp. 446–778.
[32] Liu, Y., and Yue, D. K. P., "On the Solution near the Critical Frequency for an Oscillating and Translating Body in or near a Free Surface," *Journal of Fluid Mechanics*, Vol. 254, 1993, pp. 251–266.
[33] Palm, E., and Grue, J., "On the Wave Field due to a Moving Body Performing Oscillations in the Vicinity of the Critical Frequency," *Journal of Engineering Mathematics*, Vol. 35, 1999, pp. 219–232.
[34] von Kármán, T., and Burgess, J., *General Aerodynamic Theory—Perfect Fluids. Aerodynamic Theory*, edited by W. Durand, Vol. 2, Springer–Verlag, Berlin, 1935, pp. 346–349.

A. Plotkin
Associate Editor